Atmos. Chem. Phys., 22, 6773–6786, 2022
https://doi.org/10.5194/acp-22-6773-2022
© Author(s) 2022. This work is distributed under
the Creative Commons Attribution 4.0 License.

Atmospheric Chemistry and Physics
Open Access
EGU



# Measurement report: Hygroscopic growth of ambient fine particles measured at five sites in China

**Lu Chen[1], Fang Zhang[2], Dongmei Zhang[1], Xinming Wang[3], Wei Song[3], Jieyao Liu[1], Jingye Ren[1], Sihui Jiang[1], Xue Li[1], and Zhanqing Li[4]**

[1]College of Global Change and Earth System Science, Beijing Normal University, Beijing 100875, China
[2]Environmental Science and Engineering Research Center, School of Civil and Environmental Engineering, Harbin Institute of Technology (Shenzhen), 518055 Shenzhen, China
[3]State Key Laboratory of Organic Geochemistry, Guangzhou Institute of Geochemistry, Guangzhou 510640, China
[4]Earth System Science Interdisciplinary Center and Department of Atmospheric and Oceanic Science, University of Maryland, College Park, MD, USA

**Correspondence:** Fang Zhang (zhangfang2021@hit.edu.cn) and Zhanqing Li (zli@atmos.umd.edu)

Received: 2 November 2021 – Discussion started: 26 January 2022
Revised: 31 March 2022 – Accepted: 22 April 2022 – Published: 24 May 2022

**Abstract.** The aerosol hygroscopic growth describes the interaction between aerosols and water vapor, which varies largely, depending on the chemical composition, types, and emissions of gas precursors under diverse environments. In this study, we analyzed size-resolved hygroscopic growth measured at five field sites of China by a hygroscopic tandem differential mobility analyzer (H-TDMA). Results show that the probability density function of hygroscopic growth factor (GF-PDF) at the megacity sites of Guangzhou (GZ), Shanghai (SH), and Beijing (BG) was generally with bimodal hydrophobic and hydrophilic modes, while a unimodal hydrophilic mode was dominated at the suburb sites of Xinzhou (XZ) and Xingtai (XT) throughout the measured particle size of 40–200 nm. As a result, the more hygroscopic (MH) mode accounts for a number fraction of $>80\,\%$ at the suburb sites, compared to only 20 %–40 % for 40 nm particles at the megacity sites. Further analysis shows that the GF value increases with the aggravated $PM_{2.5}$ pollution at the sites (BG, XZ, and XT) in northern China, but that is not the case for GZ and SH, which are located in the southern regions. The distinct dependence of GF on the variations in $PM_{2.5}$ concentrations among the sites suggests the spatial variability in particle composition with the evolution of pollution events in different regions of China. Moreover, different particle hygroscopic behaviors during new particle formation (NPF) events were observed at the five sites, reflecting the distinct mechanisms of NPF in diverse atmospheric environments. By including results from more sites, we find that the aerosol particles observed at those suburb sites are basically more hygroscopic than those in megacities. However, a large variability in the hygroscopic parameter $\kappa$ at a given particle size among different sites is also observed, suggesting a complex impact from local sources and atmospheric processes. The measured dataset is helpful for improving the understanding of the formation of fine particles and the regional environmental and climate change.

Published by Copernicus Publications on behalf of the European Geosciences Union.

## 1 Introduction

Aerosol hygroscopicity is characterized by the aerosol water uptake capacity when the environmental relative humidity (RH) increases (Swietlicki et al., 1999). The particle volume increases after hygroscopic growth, which leads to increased extinction and scattering and then accelerates the reduction of atmospheric visibility (Kreidenweis and Asa-Awuku, 2014; Tang and Munkelwitz, 1994). On the other hand, when particles are in the same ambient RH conditions, those with a strong hygroscopic ability tend to produce more cloud particles, increasing the cloud lifetime and decreasing the precipitation (Kandler and Schütz, 2007; Krüger et al., 2014; Wu et al., 2013). In addition, the aerosol particles after hygroscopic growth have a distinct sedimentation position and sedimentation rate in the respiratory system compared to the dry particles, thereby inducing different health effects (Peters et al., 1997; Broday and Georgopoulos, 2001). Therefore, aerosol hygroscopicity is one of the important physicochemical properties of aerosol particles (Gasparini et al., 2004) and plays a critical role in air quality, climate, and human health. The in-depth understanding of the hygroscopic behavior of atmospheric aerosols is of great significance in many research fields.

In order to measure the aerosol hygroscopicity, a variety of instruments and techniques have been developed and employed, such as the hygroscopic tandem differential mobility analyzer (H-TDMA), cloud condensation nuclei counter (CCNC), and humidified nephelometer. Among them, CCNC gives an estimate of aerosol hygroscopicity under different supersaturations but cannot provide information of particle mixing state (Roberts and Nenes, 2005). The nephelometer measures the humidity-dependent scattering coefficient over the whole size range (Kuang et al., 2018) but cannot directly obtain the size-resolved particle hygroscopicity. While H-TDMA can not only measure the hygroscopic growth factor (GF) of size-resolved aerosols under different RH but also deduce the mixing state of the particles (McMurry et al., 1996; Weingartner et al., 2002). In addition, H-TDMA measurement is based on particle number concentration, which has unique advantages in investigating the characteristics of ultrafine-mode particles; thus, it has been widely used.

To date, a number of short-term field measurements of aerosol hygroscopic growth using the H-TDMA system have been successively carried out in the North China Plain (Massling et al., 2007, 2009; Liu et al., 2011; Wu et al., 2013, 2016; Wang et al., 2017; Zhang et al., 2017; Fan et al., 2020), the Yangtze River Delta (YRD) (Zhang et al., 2011; Ye et al., 2013; Xie et al., 2017), and the Pearl River Delta (PRD; Cheng et al., 2008; Tan et al., 2013, 2017). However, most of the studies are limited to one single site or one region. A comprehensive comparison of the aerosol hygroscopic growth behavior from multiple sites has been lacking. Based on the data of a single site, for example, it is difficult to obtain insights of how particle hygroscopicity affects air pollution and is thereby unable to accurately parameterize the relationship between the two on a larger spatial scale in models. In reality, distinct dependence of aerosol hygroscopicity on air pollution levels was found by Meier et al. (2009) and Massling et al. (2009). In addition, the particle hygroscopic growth is highly correlated with the ambient RH, particle size, chemical composition, and aerosol mixing state (Pitchford and McMurry, 1994; Tan et al., 2013; Li et al., 2016; Zhang et al., 2017, 2019), which is strongly impacted by meteorological variations, aerosol formation mechanisms, and atmospheric processes (Liu et al., 2011; Wang et al., 2017; Zhang et al., 2020), thus varying widely among the observations in diverse environments. For example, several observations in the urban atmosphere showed that an enhanced aerosol hygroscopicity and cloud condensation nuclei (CCN) activation correlate with the new particle formation (NPF) events (Lance et al., 2013; Wu et al., 2016; Liu et al., 2021), while it was observed to decrease at a mid-level mountain range (Wu et al., 2013), at an urban site (X. Wang et al., 2018), and in a forest region (Deng et al., 2018). Moreover, it has been found that the size dependence of aerosol hygroscopicity was quite different among different atmospheric environment conditions (Zhang et al., 2014, 2017; Fan et al., 2020; Tan et al., 2013; Jiang et al., 2016; Cai et al., 2017, 2018).

Therefore, an extensive and comprehensive study of spatial variations in aerosol hygroscopicity is necessary to better understand the aerosol hygroscopic behavior under different pollution conditions, and the effect of atmospheric processes (e.g., pollution evolution and NPF events) on aerosol hygroscopicity in diverse environment also needed to be fully elucidated. Aerosol hygroscopic growth is investigated here at five sites in China using measurements made with the H-TDMA system. The overall characteristics of the hygroscopic growth are firstly investigated, including a comparison of the GF-PDF, different hygroscopic modes, and the diurnal cycle among the five sites. To understand the effects of atmospheric processes on particle hygroscopicity and mixing state, the dependence of the particles hygroscopicity on the pollution evolution is explored. The particle hygroscopic behavior during NPF and non-NPF events at the five sites is also compared.

## 2 Sites and measurements

### 2.1 Sampling sites

The field campaigns, which were designed with the scientific aim of a comprehensive study of the physiochemical properties of ambient aerosols, have been conducted at five sites in China, part of which are reviewed in Li et al. (2019). The five sites, including three megacity sites, Beijing (BG; 40.05° N, 116.09° E), Shanghai (SH; 31.40° N, 121.45° E), Guangzhou (GZ; 23.01° N, 113.33° E), and two suburban sites, Xinzhou (XZ; 38.24° N, 112.43° E) and Xingtai (XT; 37.18° N, 114.37° E; Fig. 1). The Beijing site is between

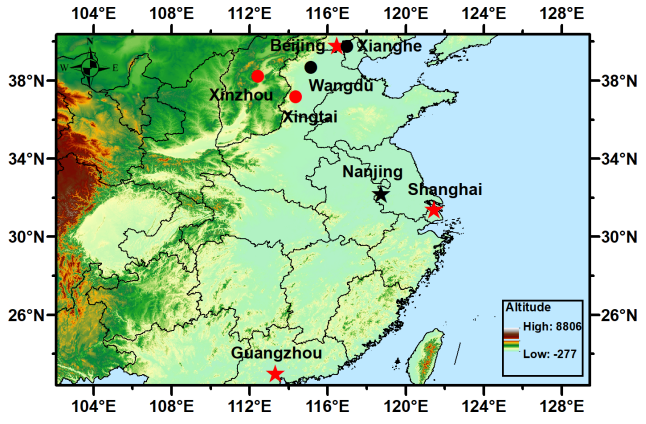


**Figure 1.** The map location of the sampling sites in this study (in red) and in previous studies (in black). The stars represent megacity sites and circles represent suburb sites. This map was made by ArcGIS (http://www.arcgis.com/index.html#, last access: 17 May 2022).

the third and fourth Ring Road in the north of Beijing, located at the meteorological tower branch of the Institute of Atmospheric Physics (IAP), Chinese Academy of Sciences, which is usually affected by local traffic and cooking emissions (Sun et al., 2015). The observation periods were from 25 May to 18 June 2017. The Shanghai site was located in the Baoshan Meteorological Bureau of Shanghai, which is near the main road (Youyi Road) with heavy traffic. So, it is mainly influenced by local emission sources from traffic and business activities that can be viewed as an urban site. The observation periods at the Shanghai site were from 6 April to 6 May 2020. The field campaign at Guangzhou site was conducted at the meteorological observation station of the Guangzhou Meteorological Bureau. The site has an altitude of 145 m, is about 120 m above the city average elevation of the PRD (Tan et al., 2017), and surrounded by a few light industrial plants and residential areas. In particular, at night, it could be affected by the cooking emissions from a nearby night market. The observation took place in November 2019. The Xinzhou air and ground observation campaign was conducted in the suburb of Xinzhou city, Shanxi province, which is located between the Lüliang and Taihang mountains and dominated by farmland without obvious emission sources nearby. Due to its high altitude, the aerosols in this area are mainly transmitted from elsewhere and are thus aged (Zhang et al., 2017). Aerosol hygroscopic growth was investigated at this site from 28 June to 22 July 2020. The experiment in Xingtai was conducted at the National Meteorological Basic Station from 1 May to 15 June 2016. This sampling site is located about 17 km northwest of the Xingtai city, the central part of the North China Plain with many heavy industrial factories nearby, such as power plants and steelworks (Y. Wang et al., 2018).

## 2.2 Instruments and methods

The H-TDMA system is custom-made and consists of two tandem differential mobility analyzers ($DMA_1$ and $DMA_2$), one water-based condensation particle counter (WCPC), and a set of humidity and temperature control devices. Before entering the instrument, the sampled aerosols first entered the Nafion dryer, reducing the RH to below 20 %. Then, the dried air flow went through a bipolar neutralizer to equilibrate the charge of the particles, after which the quasi-monodisperse particles ($D_0$, 40, 80, 110, 150, and 200 nm) were selected by the $DMA_1$. The particles entered to the $DMA_2$ through which its size increased due to higher RH ($D_p$). The humidified tube between $DMA_1$ and $DMA_2$ is controlled at RH of 90 %, with a residence time of 10 s. The hygroscopic growth factor (GF) of particles can be expressed as follows:

$$\mathrm{GF} = \frac{D_\mathrm{p}}{D_0}. \tag{1}$$

Before the measurement, the GF at different RH was determined with pure ammonium sulfate to ensure the accuracy of the H-TDMA measurement (Badger et al., 2006). The calibrations were conducted once a month. A full description of the principle, operation, and calibration of the instrument can be found in Tan et al. (2013).

We used the $\mathrm{TDMA_{inv}}$ algorithm (Gysel et al., 2009) to retrieve the actual GF probability density function (GF-PDF) from the GF measured distribution function (GF-MDF). Petters and Kreidenweis (2007) introduced the hygroscopicity parameter $\kappa$ into the $\kappa$–Köhler equation to characterize the hygroscopicity and activation capacity of aerosols, which is related to the GF and RH as follows:

$$\kappa = \left(\mathrm{GF}^3 - 1\right)\left[\frac{1}{\mathrm{RH}}\exp\left(\frac{4\sigma M_\mathrm{w}}{\mathrm{RT}\rho_\mathrm{w} D_0 \mathrm{GF}}\right) - 1\right], \tag{2}$$

where RH is the relative humidity (90 % in this study), $\sigma$ is the surface tension of the solution/air interface (here assumed to be the surface tension of pure water interface, which is about 0.0728 $\mathrm{N\,m^{-2}}$), $M_\mathrm{w}$ is the molecular weight of water ($\mathrm{kg\,mol^{-1}}$), $R$ is the universal gas constant, $T$ is the temperature (K), $\rho_\mathrm{w}$ is the density of water ($\mathrm{kg\,m^{-3}}$), and $D_0$ is the dry particle size of aerosols (m). The observed GF value was substituted into Eq. (2) to obtain the hygroscopic parameter $\kappa$.

The retrieved GF-PDF ($c(\mathrm{GF}, D_\mathrm{d})$) was normalized to unity in this study. The ensemble mean GF of GF-PDF (Sjogren et al., 2008), namely the number-weighted mean GF ($\mathrm{GF_{mean}}$), is defined as follows:

$$\mathrm{GF_{mean}} = \int_0^\infty \mathrm{GF} \times c(\mathrm{GF}, D_\mathrm{d})\mathrm{dGF}. \tag{3}$$

The corresponding ensemble mean $\kappa$ can be derived from mean GF by using Eq. (2). Because of the complex source, chemical composition, and mixing state of ambient aerosols,

different hygroscopic modes always appear in different field measurements. To better understand the hygroscopicity and mixing state of size-resolved particles, we divided them into nearly hydrophobic mode (NH; GF $\leq$ 1.21), less hygroscopic mode (LH; 1.21 < GF $\leq$ 1.37), and more hygroscopic mode (MH; GF > 1.37; Liu et al., 2011). For each mode, the number fraction (NF) can be determined from the GF-PDF as follows:

$$\mathrm{NF} = \int_{\mathrm{start}}^{\mathrm{end}} c(\mathrm{GF}, D_{\mathrm{d}})\mathrm{d}\kappa. \quad (4)$$

Apart from H-TDMA, the non-refractory chemical compositions in $PM_{2.5}$ were measured simultaneously using a quadrupole aerosol chemical speciation monitor (Q-ACSM) with a $PM_{2.5}$ aerodynamic lens in real time (Peck et al., 2016). The black carbon (BC) mass concentrations were measured using an Aethalometer (AE-33, Magee Scientific; Zhao et al., 2017). The time resolution of both Q-ACSM and AE-33 was 1 min. The particle number size distributions (PNSDs) of environmental aerosols (10–600 nm) were measured by a scanning mobility particle sizer (SMPS; TSI) with a time resolution of 5 min (Collins et al., 2002).

## 3 Results and discussion

### 3.1 Measured time series of GF-PDFs

Figure 2 shows the time series of GF-PDFs of the 40 and 150 nm particles at the five sampling sites. The white space in Fig. 2 denotes missing values or outliers caused by the instrument malfunction. In general, large variations in the GF-PDFs were observed at all the sites, showing significant temporal changes in the properties of hygroscopic growth of the fine aerosol particles. For 40 nm particles, apparent bimodal shape of strong and weak hygroscopic modes in GF-PDFs, with GF of $\sim$ 1.5 and $\sim$ 1.1, respectively, were observed at the three megacity sites (GZ, SH, and BG), while only a strong hygroscopic mode (with GF of 1.5 and 1.8) dominated the GF-PDFs at the two more rural sites (XZ and XT). This indicates the different mixing states of ambient aerosol particles between urban and non-urban regions on account of their contrasting emission sources. The urban sites are frequently influenced by local sources (e.g., traffic and cooking activities; Sun et al., 2015; Tan et al., 2017), whereas the suburban sites are relatively clean with much fewer emission sources nearby, and the aerosols are mainly transmitted from elsewhere and are thus more aged and well mixed (Zhang et al., 2017; Y. Wang et al., 2018). Owing to the continued local primary emissions in the populated regions, the freshly emitted hydrophobic ultrafine particles do not immediately mix with the background aerosol particles. As a result, the bimodal distributions of both hydrophilic and hydrophobic modes were present in GF-PDFs at the three urban sites, while the aerosol particles at the two non-urban sites are much less impacted by the local sources and more aged and internally mixed and are thus more hygroscopic.

Previous observations have also shown that the XZ site is relatively clean (Zhang et al., 2017) and has uniform aerosol chemical compositions (Wang et al., 2016). For 150 nm particles, the hygroscopic mode in the GF-PDF is basically more dominant at all the five sites, suggesting that the aerosol particles tend to be internally mixed after aging and growing in the atmosphere. The hydrophobic mode for 150 nm particles was occasionally present in the time series of GF-PDF at the BG site, due to the abundant traffic emissions and cooking sources near the site. In addition, the hydrophilic mode of 150 nm particles generally has larger GF values than that of 40 nm particles, indicating a dependence of the particle hygroscopicity on particle size, which will be further discussed in Sect. 3.6.

The campaign mean GF-PDF distributions present the hygroscopic growth properties of all measured particle diameters more clearly (Fig. 3). There were evident hydrophobic modes, particularly for 40 and 80 nm particles, at the urban sites, which are affected greatly by primary emissions (Tan et al., 2013). At the non-urban sites, however, the hydrophobic modes of GF-PDFs were much smaller throughout the whole measured sizes. The hydrophilic modes at the XZ site for each measured particle sizes were narrower and more concentrated, reflecting the uniformity of the particle compositions.

### 3.2 Diurnal variations of GF-PDFs

Figure 4 shows the diurnal variations in size-resolved GF-PDFs at these sites. In general, the diurnal variations in GF-PDFs varied largely from site to site for 40 and 80 nm particles. At these megacities where the atmosphere was heavily impacted by local primary emissions, the diurnal patterns of GF-PDFs of the small particles exhibited bimodal distributions in both hydrophobic and hydrophilic modes. The proportion of the hydrophilic modes showed an increase at around noontime (at the GZ and SH site) or early afternoon (at the BG site), with a corresponding decrease or even disappearance of the hydrophobic modes. This could be associated with the nucleation process in the daytime (Fig. S1), which demonstrated that the growth of the newly formed particles is mainly contributed by hydrophilic matters (e.g., sulfate and organic acids; Yue et al., 2010; Wu et al., 2013; Liu et al., 2021). By contrast, there is only hydrophilic mode for different sizes of the fine particles and no evident diurnal variations at the suburb site of XZ. At the XT site, the GF value of particles with different sizes in the daytime was higher than that at nighttime, but the diurnal patterns become less evident with the increase in particle size, indicating that the larger particles are more homogenously composed compared to the small ones. Overall, at the urban sites, the mean GF for 110, 150, and 200 nm particles was basically higher in the daytime than nighttime, indicating that photochemical aging

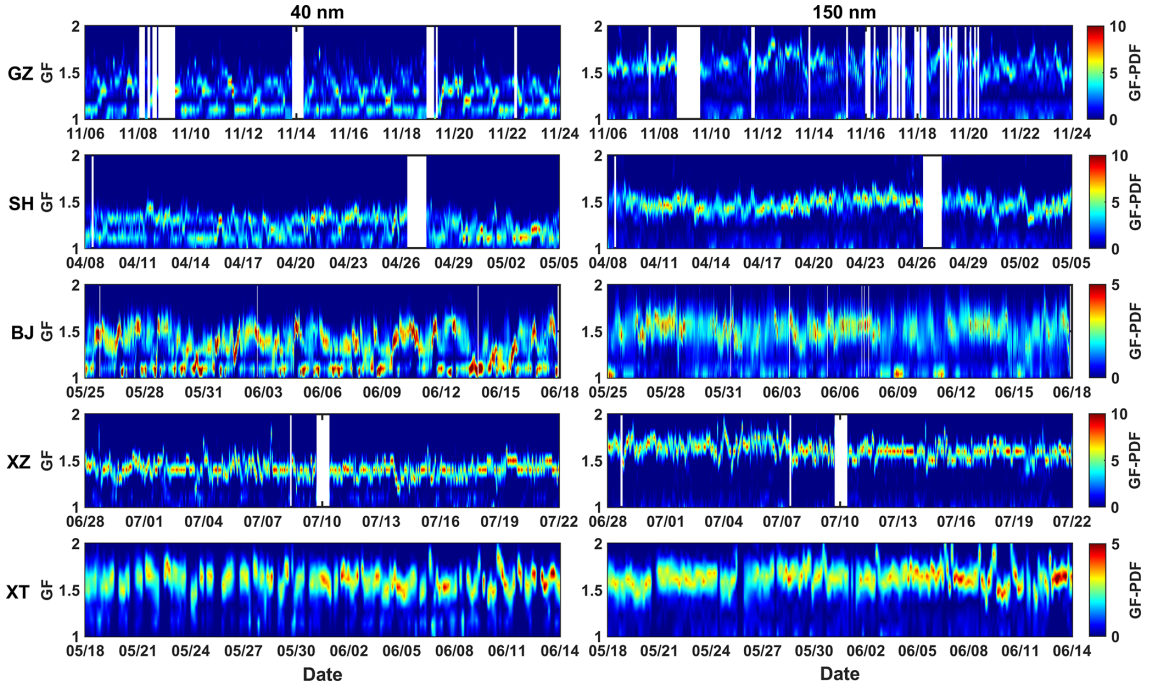


**Figure 2.** The time series of the probability density functions of growth factor (GF-PDFs) for 40 and 150 nm particles at different sampling sites (GZ, SH, BG, XZ, and XT sites). The color scales denote the GF-PDF.

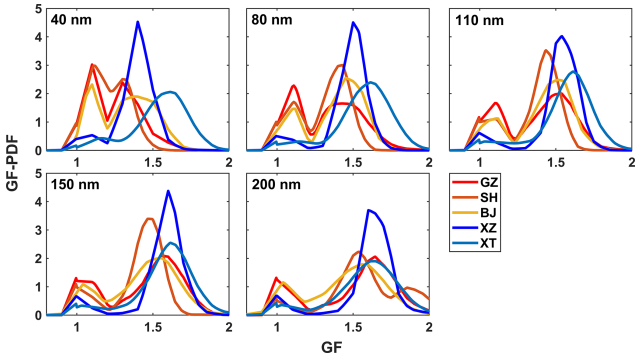


**Figure 3.** Mean probability density functions of growth factor (GF-PDFs) for different particle sizes (40–200 nm) derived from H-TDMA data at different sampling sites.

processes in the daytime enhanced the particles hygroscopicity (Wu et al., 2016; Liu et al., 2021). In addition, due to the lift of the planetary boundary layer (PBL) height after the sunrise, the aged particles above PBL could be mixed to that below PBL (Zhang et al., 2016), making the particles at all the sites more dominated by the strong hygroscopic mode.

### 3.3 Number fraction of hydrophobic, less hygroscopic, and more hygroscopic mode of the fine aerosol particles

To better understand the hygroscopicity and mixing state of size-resolved particles at the five sites, we divided the observed GF-PDFs into three modes, i.e., nearly hydrophobic mode, less hygroscopic mode, and more hygroscopic mode (Liu et al., 2011; Wang et al., 2017). The NH mode particles in submicron aerosols are mainly composed of externally mixed primary BC, primarily emitted organic matter, and their mixtures, while MH mode particles primarily consist of internally mixed hygroscopic secondary organic and inorganic matter or their mixtures with primary emissions. So, the different modes represent different aerosol composition and formation pathway. Figure 5 gives the comparison of the campaign mean number fractions of the NH, LH, and MH for 40, 80, 110, 150, and 200 nm particles at the five sites. Obviously, at the suburb sites XZ and XT, the MH modes were typically more abundant than other sites for 40 nm particles, with number fractions larger than 80 %, corresponding to the NH modes of only ∼ 10 %. At the urban sites of GZ, SH, and BG, however, NH mode accounted larger fractions of ∼ 40 %, and the values decreased with the increase in particle size. As a result, the MH modes for 40 nm particles at the urban sites only accounted for a number fraction of 20 %–40 %. On NPF days, the number fraction of MH mode at urban sites increased ∼ 4 % compared to the mean values that represent the whole measurements, and the maximum num-

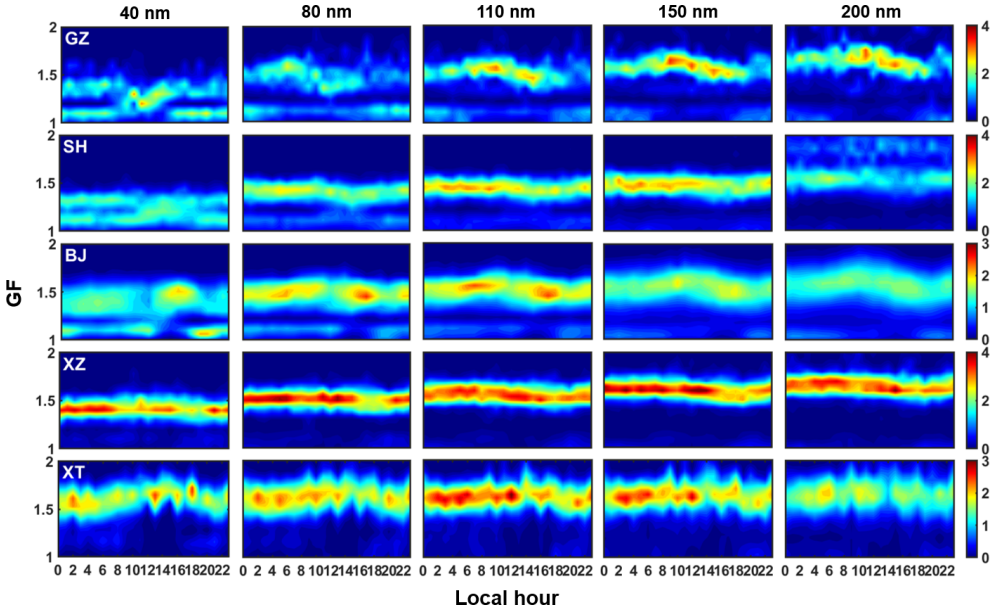


**Figure 4.** Campaign-averaged diurnal variations in GF-PDFs for all measured dry particle sizes (40–200 nm) at different sampling sites (GZ, SH, BG, XZ, and XT sites). The color scales denote the GF-PDF.

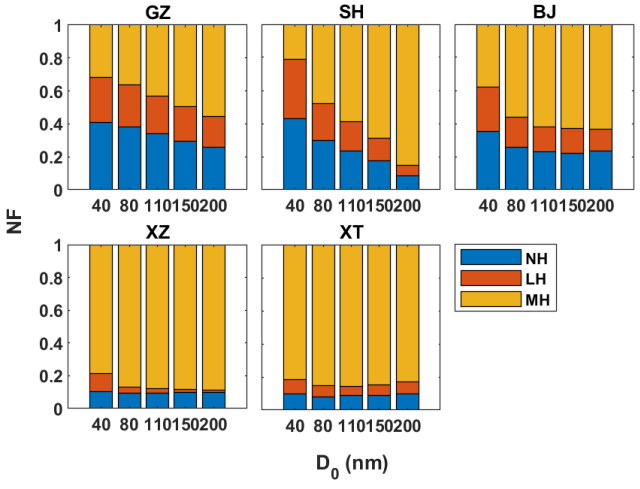


**Figure 5.** Campaign-averaged number fraction (NF) of nearly hydrophobic (NH; blue), less hygroscopic (LH; orange), and more hygroscopic (MH; yellow) groups for 40–200 nm particles at each site.

ber fraction of MH mode was ∼ 45 % at the BG site (Fig. S2). The results are basically comparable with those reported in other field campaigns in urban (e.g., Meier et al., 2009; Tan et al., 2013; Enroth et al., 2018) and suburban (e.g., Liu et al., 2011; Zhang et al., 2016; Tao et al., 2020) regions. The MH mode generally dominates at relatively remote sites where the atmosphere is less impacted by local primary sources, whereas the hydrophobic mode accounts for higher fractions at those urban sites.

### 3.4 Dependence of the particle hygroscopic properties on mass concentrations of $PM_{2.5}$

Given that the relationship between aerosol hygroscopicity and pollution levels is still unclear and varies greatly from region to region. Here, we examined and compared the dependence of the number fraction of the NH and MH mode and mean GF on $PM_{2.5}$ mass concentrations at the five sites (Figs. 6 and 7). It shows that there is no obvious dependence of number fraction of NH and MH mode on the $PM_{2.5}$ mass concentration for 40 nm particles at all the five sites, which could be expected due to the low mass fraction of ultrafine particles. In other words, this means that, whether in urban or suburban sites, the proportion of MH and NH modes of the ultrafine particles is not subject to changes in the pollution conditions. However, for accumulation mode particles of about 100–200 nm particles, with the increase in $PM_{2.5}$ mass concentration, the fraction of the MH mode roughly increased towards 1, and the fraction of the NH mode reduced to nearly 0 at the BG, XZ, and XT sites, indicating that the more particles are hygroscopic during the pollution episodes. On the contrary, the number fraction of MH mode declined slightly for 40–150 nm particles with the increase in $PM_{2.5}$ mass concentration at the GZ site, which was probably due to an increase in primary organic aerosols with the increase of pollution levels (Fig. S3). No obvious trend was observed at SH, for it is clean overall, with the $PM_{2.5}$ mass concentration being less than 60 $\mu g\,m^{-3}$ during the campaign.

Figure 7 shows that, with the increase in $PM_{2.5}$ mass concentration, there were insignificant variations in $GF_{mean}$ for 40 nm particles. The particles became more hygroscopic with

the increase of $PM_{2.5}$ mass concentration at BG, XZ, and XT. But at GZ, the aerosol particles were generally less hygroscopic with decreased $GF_{mean}$ values under higher $PM_{2.5}$. The distinct changes in aerosol particles hygroscopic behavior, with variations in $PM_{2.5}$ concentration among different sites, suggest differences in particle composition and mixing state with the evolution of pollution events in different regions of China. The results also point to different formation mechanisms or aerosol sources regulating and driving the air pollution in these regions.

### 3.5 Measured GF-PDFs of ultrafine particles during NPF and non-NPF events

In order to understand the effects of NPF on particle hygroscopic behavior, we examined the GF-PDFs of ultrafine particles during the evolutions of NPF and non-NPF events. Figure 8 displays the mean diurnal variations in PNSDs and GF-PDFs for 40 nm particles on the NPF and non-NPF days. A typical NPF event is usually with a banana-type shape that can be observed on the PNSDs, showing a sudden appearance and continuous growth of ultrafine particles (Dal et al., 2005; Wu et al., 2016). The particle size of 40 nm, which can represent the NPF-tracked particles, was thus selected. In this study, 4, 4, 8, 7, and 8 NPF events at the GZ, SH, BG, XZ, and XT sites occurred, respectively, and were selected for a further study. NPF events started at around 09:00 LT (Fig. 8a) at nearly all sites. After the onset of NPF, the hygroscopic modes in GF-PDFs at the sites of BG, XZ, and XT were obviously enhanced, corresponding to significant increases in the $GF_{mean}$ values (Fig. 8b). This suggests that the more hygroscopic chemical components were formed in the nucleation and growth processes, leading to an increase in the number fraction of the hydrophilic mode. Liu et al. (2021) showed an obvious enhanced hygroscopicity of 40 nm organic aerosol (OA) particles during NPF events in urban Beijing, and Shantz et al. (2012) and Wu et al. (2016) also observed an enhancement of the fraction of water-soluble compounds in the newly formed particles, showing that more than 40 % of 50 nm newly formed particles are water-soluble compounds. In addition, the sulfuric acid may be a dominant contributor to new particle growth in the North China Plain (Yue et al., 2010). While at the GZ site, the $GF_{mean}$ increased very slightly, at the SH site, it even declined from the beginning to the end of the NPF event, showing that the NPF processes generated less hygroscopic particles. The decreased GF of the nucleated particles would also relate to the chemical component participating in the nucleating and growth processes. It is likely that those hydrophobic secondary organic aerosols (SOAs; with GF of $\sim 1.1$ at 90 % RH; Kulmala et al., 2013) may play an important role in the growth process of the newly formed particles at GZ and SH sites. This result is also consistent with the previous study performed in clean environments, where the newly formed particles consisted of a minor fraction of water-soluble fraction, and the GF value of the newly formed particles decreased with the particle growth (Wu et al., 2013; Kawana et al., 2017; Li et al., 2017). Compared to NPF days, no significant elevations on non-NPF days were observed in $GF_{mean}$ in the daytime at all the sites (Fig. 8d and e), further demonstrating the effect of NPF on the particles hygroscopicity. On non-NPF days, the 40 nm particles are mainly from the local primary sources (cooking, traffic, etc.), which can be indicated from the measured peak particle number concentration during the rush hours or at lunch- and dinnertime (Fig. 8c). This is also illustrated by the diurnal variation in the size-resolved chemical components measured at BG, showing that the mass fraction of cooking organic aerosols (COAs) and traffic-related hydrocarbon organic aerosols (HOAs) increased obviously during rush hour and at lunch- and dinnertime on non-NPF days (Sun et al., 2016, 2018). The XZ site is near the main road and, thus, is more affected by the traffic emissions, including road truck emissions at night (Fig. 8c), while the catering night market activities near the GZ site, which continue until the next morning, lead to a large number of small particle emissions. The distinct changes in aerosol particle hygroscopic behavior at the sites indicate that different compositions of the nucleated particles in different regions of China, which further reflect different formation mechanisms regulating the new particle formation in diverse atmospheric environment.

Also, the $GF_{mean}$ of the 40 nm particles on NPF days is generally greater than particles with the same sizes during non-NPF days (Fig. 9), further confirming the role of nucleation process on enhancing the particle hygroscopicity. For accumulation mode particles, the $GF_{mean}$ values during non-NPF days are overall higher than that on NPF days at the BG, XZ, and XT sites, due to the larger particles probably being from secondary conversion and primarily being composed of more hygroscopic substances on non-NPF days. But, at the GZ and SH sites, the $GF_{mean}$ values for larger particles are lower during non-NPF days, suggesting that there are primary sources of the accumulation mode particles at the two sites.

### 3.6 Comparison of size-resolved hygroscopic parameter ($\kappa$) of fine aerosol particles observed at different sites

To further investigate the spatial variability in the aerosol hygroscopicity in different regions of China, we presented campaign mean size-resolved $\kappa$ for NH, LH, and MH modes calculated from the H-TDMA measurements of the five sites (Fig. 10a). The measured bulk mass concentration fraction of chemical components in $PM_{2.5}$ measured by the ACSM is also presented here (Fig. 10b). Clearly, it shows that the MH mode particles hygroscopicity was closely relevant to the chemical compositions. That is, the particles were found to be more hygroscopic with larger $\kappa$ values at the sites such as BG, XZ, and XT, where the hygroscopic inorganics ac-

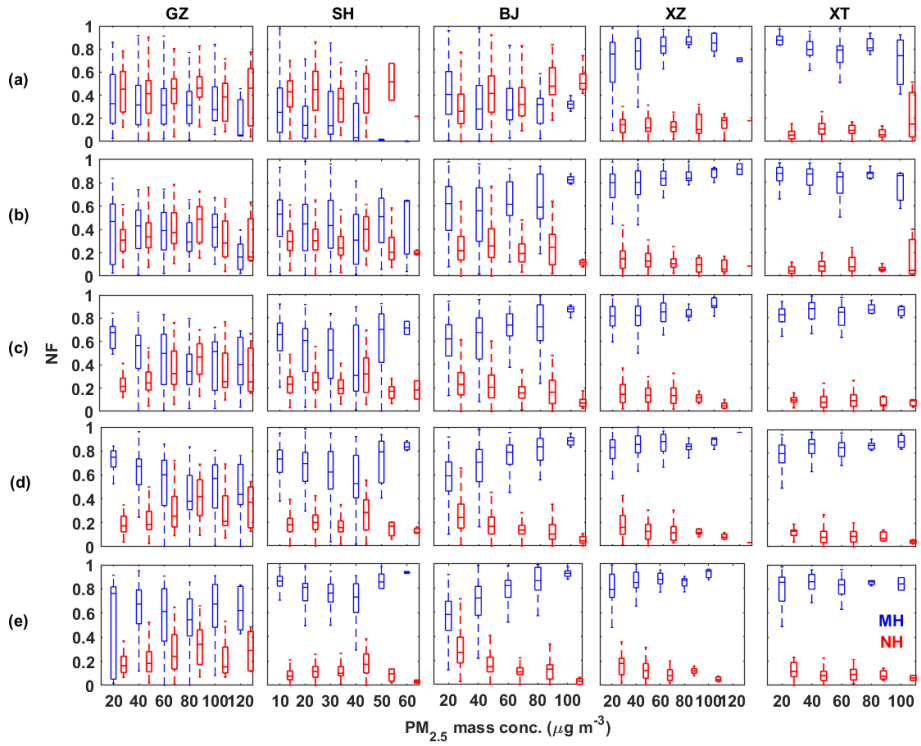


**Figure 6.** Box diagram for the number fraction of nearly hydrophobic (NH) mode (red) and more hygroscopic (MH) mode (blue) of **(a–e)** all selected diameter particles (40–200 nm) under different $PM_{2.5}$ mass concentrations from all sampling sites. The horizontal line in the block diagram represents the median, the upper and lower borders represent the 25th and 75th percentiles, and the upper and lower borders of the dotted vertical line represent the 10th and 90th percentiles.

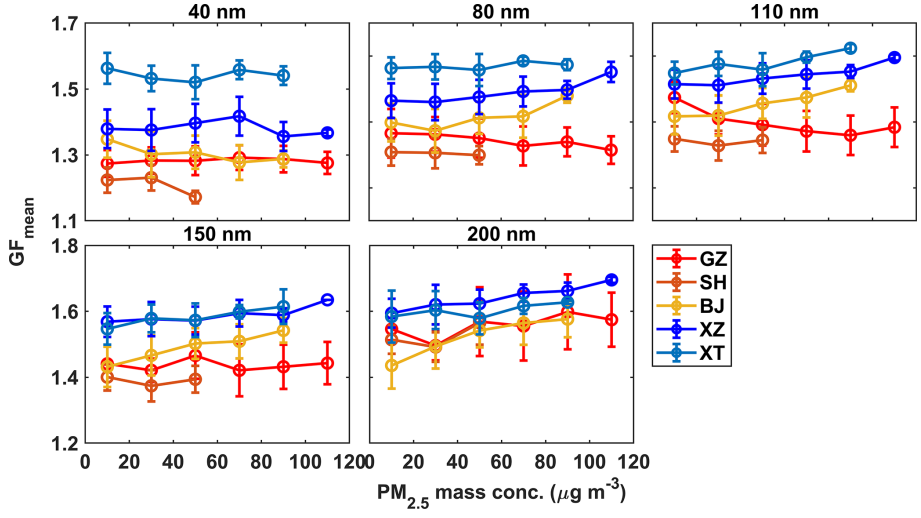


**Figure 7.** The mean value of number-weighted mean growth factor ($GF_{mean}$) of all selected diameter particles (40–200 nm) under different $PM_{2.5}$ mass concentrations from all sampling sites.

count for a large mass fraction in $PM_{2.5}$, while they were less hygroscopic when the organics dominated the chemical composition at the sites of GZ and SH. This is also demonstrated by comparing a whole time series of the mass fraction of chemical composition with the $\kappa$ at the five sites (Fig. S4), showing that the $\kappa$ generally increases with increase of the mass fraction of hydrophilic inorganic salts, and the opposite is true for organics. Previously, quite a weak hygroscopicity of organic materials (with $GF_{org}$ ranging between 1 and 1.1) has been observed at GZ (Hong et al., 2018), whereas

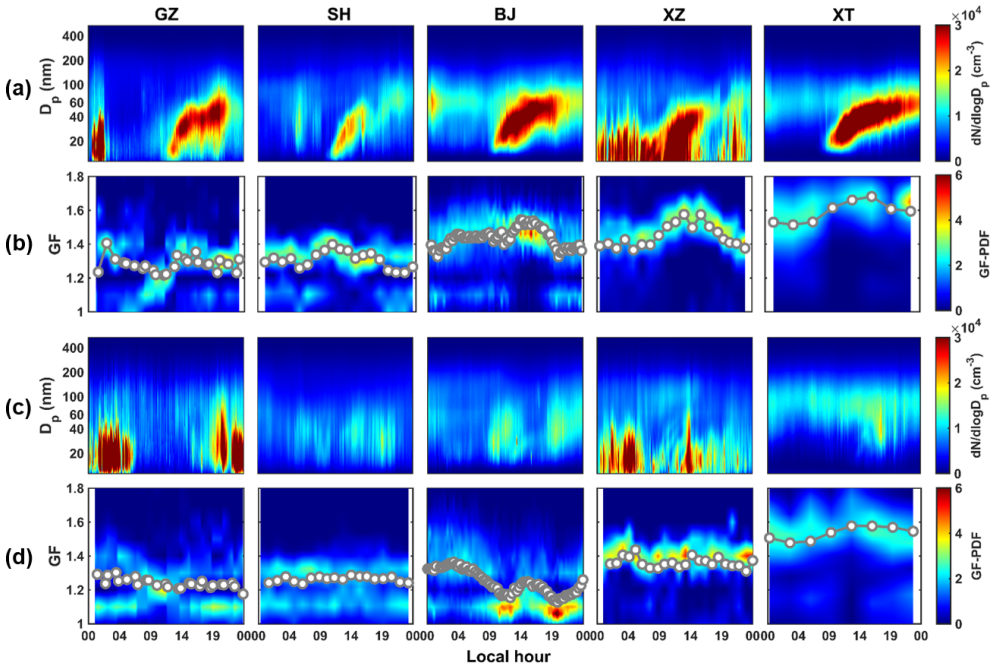


**Figure 8.** The mean variation in particle number size distributions (PNSDs) and the probability distribution functions of growth factor (GF-PDFs) for 40 nm particles during **(a–b)** NPF and **(c–d)** non-NPF days at the five sampling sites. The dots in panels **(b)** and **(d)** represent the $GF_{mean}$ values.

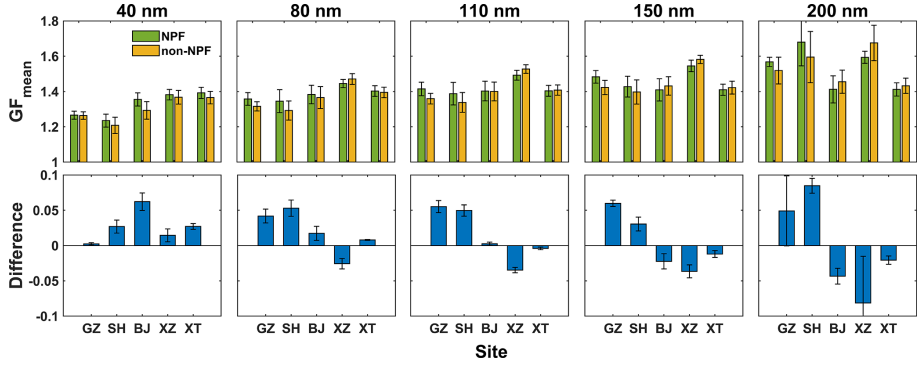


**Figure 9.** The mean values and differences in number-weighted mean growth factor ($GF_{mean}$) during NPF and non-NPF days for particles with the size of 40–200 nm from all sampling sites. The difference represents the $GF_{mean}$ of NPF days minus the $GF_{mean}$ of non-NPF days.

the greater $\kappa$ values at BG were not only caused by the high mass fraction of hygroscopic inorganic salts (e.g., sulfate and nitrate) in $PM_{2.5}$ but also because the organics were demonstrated to be more hygroscopic with mean $\kappa$ values of $\sim$0.28 in urban Beijing (Liu et al., 2021). The mean $\kappa$ values of NH and LH mode are close to 0 at the five sites and decrease slightly with the increase in particle size. Figure 10c shows a comparison of size-dependent $\kappa$ values reported in previous studies and that observed in this study. Generally, the mean $\kappa$ values of the particles at all measured sizes are greater in suburban regions (Zhang et al., 2016; Wang et al., 2017) compared to those of measured in megacities (Tan et al., 2013; Ye et al., 2013; Xu et al., 2015; Jiang et al., 2016; Wu et al., 2016). This is consistent with that observed at the five sites by this study. However, it exhibits a wide and large variability in $\kappa$ values among different sites at a given $D_p$. The large spatial difference in $\kappa$ values suggests that there are different emission sources and complex atmospheric physical and chemical processes which could be significantly different under diverse ambient conditions. This is particularly true for the particles with a small size. Note that the $\kappa$ values observed at the five sites are more consistent for 200 nm particles, which is owing to the fact that the larger particles are normally more aged and with homogenous compositions (Y. Wang et al., 2018).

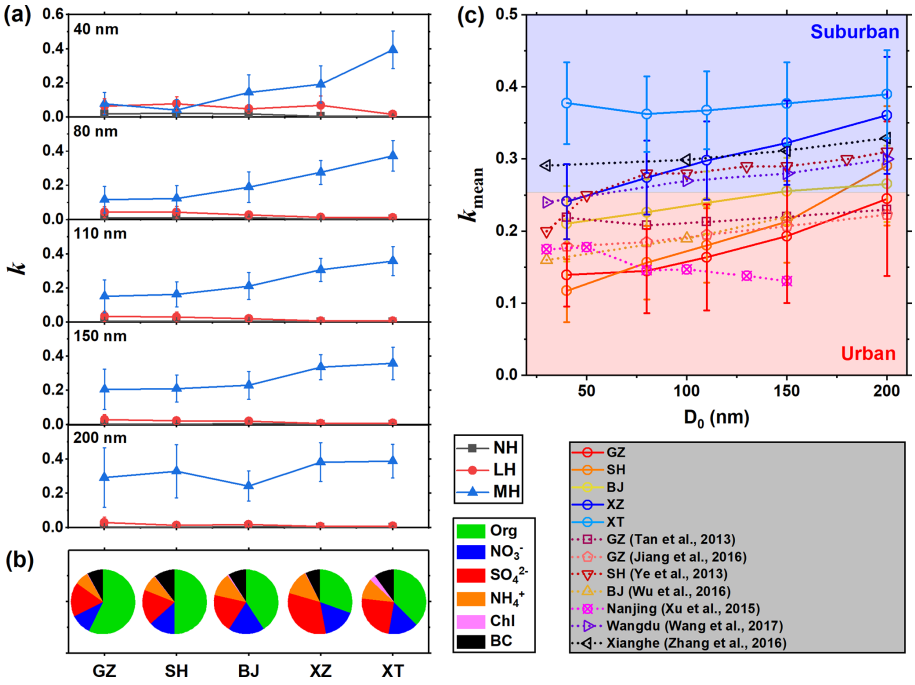


**Figure 10.** **(a)** Size-resolved mean hygroscopicity parameters ($\kappa$) that are nearly hydrophobic (NH), less hygroscopic (LH), and more hygroscopic (MH) for all measured particle sizes at different sites. **(b)** Campaign-averaged bulk mass fraction of chemical compositions of $PM_{2.5}$. The BC mass concentration of the GZ site is based on the data measured in January 2020 due to the lack of observations in November 2019. **(c)** Size-dependent mean $\kappa$ for all measured particle sizes retrieved from the H-TDMA measurements at different sites and reported by previous studies (Tan et al., 2013; Jiang et al., 2016; Ye et al., 2013; Wu et al., 2016; Xu et al., 2015; Wang et al., 2017; Zhang et al., 2016). The error bars represent $\pm 1\sigma$.

## 4 Conclusion

In this study, the hygroscopic growth factors at five sites, including three urban and two non-urban sites across China, were investigated to understand the characteristics and the impact of mixing states of aerosols under diverse environmental conditions. The study made use of comprehensive measurements of size-resolved particles (40–200 nm) at RH of 90 % made with a H-TDMA system, combined with the chemical composition and particle number size distribution measured by a ACSM and a SMPS, respectively. There exist hydrophobic modes of GF-PDFs at the GZ, SH, and BG sites for small particles, and the unimodal hydrophilic modes throughout the whole measured sizes are dominant at the XZ and XT sites. The more hygroscopic mode (MH) mode was typically more abundant at the XZ and XT site, with a corresponding number fractions of $>80$ %, indicating that the particles at suburban sites were highly aged and internally mixed. The number fractions of MH modes for 40 nm particles account for only 20 %–40 % at those urban sites of GZ, SH, and BG. The diurnal patterns of GF-PDF at the megacity sites of GZ, SH, and BG show obvious enhancement of the proportion of hydrophilic modes in daytime; however, such patterns are absent at the suburb sites of XZ and XT. Further analysis reveals that the aggregated $PM_{2.5}$ pollution leads to more hygroscopic particles at the sites in north China (BG, XZ, and XT), but that is not the case in the southern sites (GZ and SH). The distinct dependence of aerosol hygroscopicity on $PM_{2.5}$ concentrations among the sites is attributed to the spatial variability in particle formation mechanisms with the evolution of pollution events in different regions of China. Moreover, the particle hygroscopicity during NPF and non-NPF days at each site was also investigated. The distinct particles hygroscopic behaviors during NPF events are observed at the five sites, demonstrating the different mechanisms of NPF in diverse atmospheric environment. There was no obvious variation in particle hygroscopicity observed during non-NPF days at all the five sites.

Overall, the aerosol particles observed at the suburban sites are more hygroscopic than those of in megacities, but note that a wide and large variability in the hygroscopic parameter $\kappa$ among different sites at a given particle size suggests the complex impact from emission sources and atmospheric physical and chemical processes. Future field measurements and observations should be conducted at more sites with a longer duration, so as to improve understanding of the formation of fine particles and the impact on regional environment and climate change. In addition, it is worth noting that measurements at the SH and XZ site were conducted during COVID-19, when the gaseous pollutants and chemi-

cal composition of aerosols might be affected to varying degrees. This would thereby lead to changes in the particle mixing state and hygroscopicity. For example, in North China, the study has shown that the secondary process or atmospheric oxidation were enhanced during the COVID-19 pandemic, likely yielding more hygroscopic species like aqueous secondary organic aerosol (Zhong et al., 2021). Whereas, in Yangtze River Delta, the study has shown that the secondary components decreased during the lockdown (Ma et al., 2021). However, the evaluation of such effect of the pandemic on aerosols' hygroscopicity is complex, owing to variation in the meteorological conditions, emissions, and anthropogenic sources with seasons and years. It warrants further studies to clarify such impact in the future.

**Data availability.** All data needed to evaluate the conclusions in the paper are present in the Sect. 3 and/or the Supplement. Also, all data used in the study are available from the corresponding author upon request (zhangfang2021@hit.edu.cn).

**Supplement.** The supplement related to this article is available online at: https://doi.org/10.5194/acp-22-6773-2022-supplement.

**Author contributions.** FZ conceived the conceptual development of the paper. FZ, ZL, and LC directed and performed the experiments with DZ, JL, SJ, JR, XW, WS, and XL, and FZ and LC conducted the data analysis and wrote the draft. All authors edited and commented on the various sections of the paper.

**Competing interests.** The contact author has declared that neither they nor their co-authors have any competing interests.

**Disclaimer.** Publisher's note: Copernicus Publications remains neutral with regard to jurisdictional claims in published maps and institutional affiliations.

**Acknowledgements.** This work has been funded by the National Basic Research Program of China (grant no. 2017YFC1501702), the NSFC research projects (grant nos. 41975174 and 41675141), and BNU Interdisciplinary Research Foundation for the First-Year Doctoral Candidates (grant no. BNUXKJC2126). We thank all participants in the field campaigns, for their tireless work and cooperation.

**Financial support.** This research has been supported by the National Defense Basic Scientific Research Program of China (grant no. 2017YFC1501702), the National Natural Science Foundation of China (grant nos. 41975174 and 41675141), and the BNU Interdisciplinary Research Foundation for the First-Year Doctoral Candidates (grant no. BNUXKJC2126).

**Review statement.** This paper was edited by Alex Lee and reviewed by two anonymous referees.

## References

Badger, C. L., George, I., Griffiths, P. T., Braban, C. F., Cox, R. A., and Abbatt, J. P. D.: Phase transitions and hygroscopic growth of aerosol particles containing humic acid and mixtures of humic acid and ammonium sulphate, Atmos. Chem. Phys., 6, 755–768, https://doi.org/10.5194/acp-6-755-2006, 2006.

Broday, D. M. and Georgopoulos, P. G.: Growth and Deposition of Hygroscopic Particulate Matter in the Human Lungs, Aerosol Sci. Technol., 34, 144–159, https://doi.org/10.1080/02786820118725, 2001.

Cai, M., Tan, H., Chan, C. K., Mochida, M., Hatakeyama, S., Kondo, Y., Schurman, M. I., Xu, H., Li, F., Shimada, K., Li, L., Deng, Y., Yai, H., Matsuki, A., Qin, Y., and Zhao, J.: Comparison of aerosol hygroscopcity, volatility, and chemical composition between a suburban site in the Pearl River Delta region and a marine site in Okinawa, Aerosol Air Qual. Res., 17, 3194–3208, https://doi.org/10.4209/aaqr.2017.01.0020, 2017.

Cai, M., Tan, H., Chan, C. K., Qin, Y., Xu, H., Li, F., Schurman, M. I., Liu, L., and Zhao, J.: The size-resolved cloud condensation nuclei (CCN) activity and its prediction based on aerosol hygroscopicity and composition in the Pearl Delta River (PRD) region during wintertime 2014, Atmos. Chem. Phys., 18, 16419–16437, https://doi.org/10.5194/acp-18-16419-2018, 2018.

Cheng, Y. F., Wiedensohler, A., Eichler, H., Heintzenberg, J., Tesche, M., Ansmann, A., Wendisch, M., Su, H., Althausen, D., Herrmann, H., Gnauk, T., Brüggemann, E., Hu, M., and Zhang, Y. H.: Relative humidity dependence of aerosol optical properties and direct radiative forcing in the surface boundary layer at Xinken in Pearl River Delta of China: An observation based numerical study, Atmos. Environ., 42, 6373–6397, https://doi.org/10.1016/j.atmosenv.2008.04.009, 2008.

Collins, D. R., Flagan, R. C., and Seinfeld, J. H.: Improved Inversion of Scanning DMA Data, Aerosol Sci. Tech., 36, 1–9, https://doi.org/10.1080/027868202753339032, 2002.

Dal Maso, M., Kulmala, M., Riipinen, I., Wagner, R., Hussein, T., Aalto, P. P., and Lehtinen, K. E. J.: Formation and growth of fresh atmospheric aerosols: eight years of aerosol size distribution data from SMEAR II, Hyytiälä, Finland, Boreal Environ. Res., 10, 323–336, 2005.

Deng, Y., Kagami, S., Ogawa, S., Kawana, K., Nakayama, T., Kubodera, R., Adachi, K., Hussein, T., Miyazaki, Y., and Mochida, M.: Hygroscopicity of Organic Aerosols and Their Contributions to CCN Concentrations Over a Midlatitude Forest in Japan, J. Geophys. Res.-Atmos., 123, 9703–9723, https://doi.org/10.1029/2017JD027292, 2018.

Enroth, J., Mikkilä, J., Németh, Z., Kulmala, M., and Salma, I.: Wintertime hygroscopicity and volatility of ambient urban aerosol particles, Atmos. Chem. Phys., 18, 4533–4548, https://doi.org/10.5194/acp-18-4533-2018, 2018.

Fan, X., Liu, J., Zhang, F., Chen, L., Collins, D., Xu, W., Jin, X., Ren, J., Wang, Y., Wu, H., Li, S., Sun, Y., and Li, Z.: Contrasting size-resolved hygroscopicity of fine particles derived by HTDMA and HR-ToF-AMS measurements between summer and winter in Beijing: the impacts of aerosol ag-

ing and local emissions, Atmos. Chem. Phys., 20, 915–929, https://doi.org/10.5194/acp-20-915-2020, 2020.

Gasparini, R., Li, R., and Collins, D. R.: Integration of size distributions and size-resolved hygroscopicity measured during the Houston Supersite for compositional categorization of the aerosol, Atmos. Environ., 38, 3285–3303, https://doi.org/10.1016/j.atmosenv.2004.03.019, 2004.

Gysel, M., McFiggans, G. B., and Coe, H.: Inversion of tandem differential mobility analyser (TDMA) measurements, J. Aerosol Sci., 40, 134–151, https://doi.org/10.1016/j.jaerosci.2008.07.013, 2009.

Hong, J., Xu, H., Tan, H., Yin, C., Hao, L., Li, F., Cai, M., Deng, X., Wang, N., Su, H., Cheng, Y., Wang, L., Petäjä, T., and Kerminen, V.-M.: Mixing state and particle hygroscopicity of organic-dominated aerosols over the Pearl River Delta region in China, Atmos. Chem. Phys., 18, 14079–14094, https://doi.org/10.5194/acp-18-14079-2018, 2018.

Jiang, R., Tan, H., Tang, L., Cai, M., Yin, Y., Li, F., Liu, L., Xu, H., Chan, P. W., Deng, X., and Wu, D.: Comparison of aerosol hygroscopicity and mixing state between winter and summer seasons in Pearl River Delta region, China, Atmos. Res., 169, 160–170, https://doi.org/10.1016/j.atmosres.2015.09.031, 2016.

Kandler, K. and Schütz, L.: Climatology of the average water-soluble volume fraction of atmospheric aerosol, Atmos. Res., 83, 77–92, https://doi.org/10.1016/j.atmosres.2006.03.004, 2007.

Kawana, K., Nakayama, T., Kuba, N., and Mochida, M.: Hygroscopicity and cloud condensation nucleus activity of forest aerosol particles during summer in Wakayama, Japan, J. Geophys. Res.-Atmos., 122, 3042–3064, https://doi.org/10.1002/2016JD025660, 2017.

Kreidenweis, S. M. and Asa-Awuku, A.: 5.13 – Aerosol Hygroscopicity: Particle Water Content and Its Role in Atmospheric Processes, in: Treatise on Geochemistry, second edn., edited by: Holland, H. D. and Turekian, K. K., Elsevier, Oxford, 331–361, https://doi.org/10.1016/B978-0-08-095975-7.00418-6, 2014.

Krüger, M. L., Mertes, S., Klimach, T., Cheng, Y. F., Su, H., Schneider, J., Andreae, M. O., Pöschl, U., and Rose, D.: Assessment of cloud supersaturation by size-resolved aerosol particle and cloud condensation nuclei (CCN) measurements, Atmos. Meas. Tech., 7, 2615–2629, https://doi.org/10.5194/amt-7-2615-2014, 2014.

Kuang, Y., Zhao, C. S., Zhao, G., Tao, J. C., Xu, W., Ma, N., and Bian, Y. X.: A novel method for calculating ambient aerosol liquid water content based on measurements of a humidified nephelometer system, Atmos. Meas. Tech., 11, 2967–2982, https://doi.org/10.5194/amt-11-2967-2018, 2018.

Kulmala, M., Kontkanen, J., Junninen, H., Lehtipalo, K., Manninen Hanna, E., Nieminen, T., Petäjä, T., Sipilä, M., Schobesberger, S., Rantala, P., Franchin, A., Jokinen, T., Järvinen, E., Äijälä, M., Kangasluoma, J., Hakala, J., Aalto Pasi, P., Paasonen, P., Mikkilä, J., Vanhanen, J., Aalto, J., Hakola, H., Makkonen, U., Ruuskanen, T., Mauldin Roy, L., Duplissy, J., Vehkamäki, H., Bäck, J., Kortelainen, A., Riipinen, I., Kurtén, T., Johnston Murray, V., Smith James, N., Ehn, M., Mentel Thomas, F., Lehtinen Kari, E. J., Laaksonen, A., Kerminen, V.-M., and Worsnop, D. R.: Direct Observations of Atmospheric Aerosol Nucleation, Science, 339, 943–946, https://doi.org/10.1126/science.1227385, 2013.

Lance, S., Raatikainen, T., Onasch, T. B., Worsnop, D. R., Yu, X.-Y., Alexander, M. L., Stolzenburg, M. R., McMurry, P. H., Smith, J. N., and Nenes, A.: Aerosol mixing state, hygroscopic growth and cloud activation efficiency during MIRAGE 2006, Atmos. Chem. Phys., 13, 5049–5062, https://doi.org/10.5194/acp-13-5049-2013, 2013.

Li, W., Sun, J., Xu, L., Shi, Z., Riemer, N., Sun, Y., Fu, P., Zhang, J., Lin, Y., Wang, X., Shao, L., Chen, J., Zhang, X., Wang, Z., and Wang, W.: A conceptual framework for mixing structures in individual aerosol particles, J. Geophys. Res.-Atmos., 121, 13784–13798, https://doi.org/10.1002/2016JD025252, 2016.

Li, Y., Zhang, F., Li, Z., Sun, L., Wang, Z., Li, P., Sun, Y., Ren, J., Wang, Y., Cribb, M., and Yuan, C.: Influences of aerosol physiochemical properties and new particle formation on CCN activity from observation at a suburban site of China, Atmos. Res., 188, 80–89, https://doi.org/10.1016/j.atmosres.2017.01.009, 2017.

Li, Z., Wang, Y., Guo, J., Zhao, C., Cribb, M. C., Dong, X., Fan, J., Gong, D., Huang, J., Jiang, M., Jiang, Y., Lee, S. S., Li, H., Li, J., Liu, J., Qian, Y., Rosenfeld, D., Shan, S., Sun, Y., Wang, H., Xin, J., Yan, X., Yang, X., Yang, X.-Q., Zhang, F., and Zheng, Y.: East Asian Study of Tropospheric Aerosols and their Impact on Regional Clouds, Precipitation, and Climate ($\text{EAST-AIR}_{\text{CPC}}$), J. Geophys. Res.-Atmos., 124, 13026–13054, https://doi.org/10.1029/2019JD030758, 2019.

Liu, J., Zhang, F., Xu, W., Sun, Y., Chen, L., Li, S., Ren, J., Hu, B., Wu, H., and Zhang, R.: Hygroscopicity of Organic Aerosols Linked to Formation Mechanisms, 48, e2020GL091683, https://doi.org/10.1029/2020GL091683, 2021.

Liu, P. F., Zhao, C. S., Göbel, T., Hallbauer, E., Nowak, A., Ran, L., Xu, W. Y., Deng, Z. Z., Ma, N., Mildenberger, K., Henning, S., Stratmann, F., and Wiedensohler, A.: Hygroscopic properties of aerosol particles at high relative humidity and their diurnal variations in the North China Plain, Atmos. Chem. Phys., 11, 3479–3494, https://doi.org/10.5194/acp-11-3479-2011, 2011.

Ma, J., Shen, J., Wang, P., Zhu, S., Wang, Y., Wang, P., Wang, G., Chen, J., and Zhang, H.: Modeled changes in source contributions of particulate matter during the COVID-19 pandemic in the Yangtze River Delta, China, Atmos. Chem. Phys., 21, 7343–7355, https://doi.org/10.5194/acp-21-7343-2021, 2021.

Massling, A., Leinert, S., Wiedensohler, A., and Covert, D.: Hygroscopic growth of sub-micrometer and one-micrometer aerosol particles measured during ACE-Asia, Atmos. Chem. Phys., 7, 3249–3259, https://doi.org/10.5194/acp-7-3249-2007, 2007.

Massling, A., Stock, M., Wehner, B., Wu, Z. J., Hu, M., Brüggemann, E., Gnauk, T., Herrmann, H., and Wiedensohler, A.: Size segregated water uptake of the urban submicrometer aerosol in Beijing, Atmos. Environ., 43, 1578–1589, https://doi.org/10.1016/j.atmosenv.2008.06.003, 2009.

McMurry, P. H., Litchy, M., Huang, P.-F., Cai, X., Turpin, B. J., Dick, W. D., and Hanson, A.: Elemental composition and morphology of individual particles separated by size and hygroscopicity with the TDMA, Atmos. Environ., 30, 101–108, https://doi.org/10.1016/1352-2310(95)00235-Q, 1996.

Meier, J., Wehner, B., Massling, A., Birmili, W., Nowak, A., Gnauk, T., Brüggemann, E., Herrmann, H., Min, H., and Wiedensohler, A.: Hygroscopic growth of urban aerosol particles in Beijing (China) during wintertime: a comparison of three experimental methods, Atmos. Chem. Phys., 9, 6865–6880, https://doi.org/10.5194/acp-9-6865-2009, 2009.

Peck, J., Gonzalez, L. A., Williams, L. R., Xu, W., Croteau, P. L., Timko, M. T., Jayne, J. T., Worsnop, D. R., Miake-Lye, R. C., and Smith, K. A.: Development of an aerosol mass spectrom-

eter lens system for $PM_{2.5}$, Aerosol Sci. Tech., 50, 781–789, https://doi.org/10.1080/02786826.2016.1190444, 2016.

Peters, A., Wichmann, H. E., Tuch, T., and Heyder, J.: Respiratory effects are associated with the number of ultrafine particles, Am. J. Respir. Crit. Care Med., 155, 1376–1383, https://doi.org/10.1164/ajrccm.155.4.9105082, 1997.

Petters, M. D. and Kreidenweis, S. M.: A single parameter representation of hygroscopic growth and cloud condensation nucleus activity, Atmos. Chem. Phys., 7, 1961–1971, https://doi.org/10.5194/acp-7-1961-2007, 2007.

Pitchford, M. L. and McMurry, P. H.: Relationship between measured water vapor growth and chemistry of atmospheric aerosol for Grand Canyon, Arizona, in winter 1990, Atmos. Environ., 28, 827–839, https://doi.org/10.1016/1352-2310(94)90242-9, 1994.

Roberts, G. C. and Nenes, A.: A Continuous-Flow Streamwise Thermal-Gradient CCN Chamber for Atmospheric Measurements, Aerosol Sci. Tech., 39, 206–221, https://doi.org/10.1080/027868290913988, 2005.

Shantz, N. C., Pierce, J. R., Chang, R. Y. W., Vlasenko, A., Riipinen, I., Sjostedt, S., Slowik, J. G., Wiebe, A., Liggio, J., Abbatt, J. P. D., and Leaitch, W. R.: Cloud condensation nuclei droplet growth kinetics of ultrafine particles during anthropogenic nucleation events, Atmos. Environ., 47, 389–398, https://doi.org/10.1016/j.atmosenv.2011.10.049, 2012.

Sjogren, S., Gysel, M., Weingartner, E., Alfarra, M. R., Duplissy, J., Cozic, J., Crosier, J., Coe, H., and Baltensperger, U.: Hygroscopicity of the submicrometer aerosol at the high-alpine site Jungfraujoch, 3580 m a.s.l., Switzerland, Atmos. Chem. Phys., 8, 5715–5729, https://doi.org/10.5194/acp-8-5715-2008, 2008.

Sun, Y., Du, W., Fu, P., Wang, Q., Li, J., Ge, X., Zhang, Q., Zhu, C., Ren, L., Xu, W., Zhao, J., Han, T., Worsnop, D. R., and Wang, Z.: Primary and secondary aerosols in Beijing in winter: sources, variations and processes, Atmos. Chem. Phys., 16, 8309–8329, https://doi.org/10.5194/acp-16-8309-2016, 2016.

Sun, Y., Xu, W., Zhang, Q., Jiang, Q., Canonaco, F., Prévôt, A. S. H., Fu, P., Li, J., Jayne, J., Worsnop, D. R., and Wang, Z.: Source apportionment of organic aerosol from 2-year highly time-resolved measurements by an aerosol chemical speciation monitor in Beijing, China, Atmos. Chem. Phys., 18, 8469–8489, https://doi.org/10.5194/acp-18-8469-2018, 2018.

Sun, Y. L., Wang, Z. F., Du, W., Zhang, Q., Wang, Q. Q., Fu, P. Q., Pan, X. L., Li, J., Jayne, J., and Worsnop, D. R.: Long-term real-time measurements of aerosol particle composition in Beijing, China: seasonal variations, meteorological effects, and source analysis, Atmos. Chem. Phys., 15, 10149–10165, https://doi.org/10.5194/acp-15-10149-2015, 2015.

Swietlicki, E., Zhou, J., Berg, O. H., Martinsson, B. G., Frank, G., Cederfelt, S.-I., Dusek, U., Berner, A., Birmili, W., Wiedensohler, A., Yuskiewicz, B., and Bower, K. N.: A closure study of sub-micrometer aerosol particle hygroscopic behavior, Atmos. Res., 50, 205–240, https://doi.org/10.1016/S0169-8095(98)00105-7, 1999.

Tan, H., Yin, Y., Gu, X., Li, F., Chan, P. W., Xu, H., Deng, X., and Wan, Q.: An observational study of the hygroscopic properties of aerosols over the Pearl River Delta region, Atmos. Environ., 77, 817–826, https://doi.org/10.1016/j.atmosenv.2013.05.049, 2013.

Tan, H., Cai, M., Fan, Q., Liu, L., Li, F., Chan, P. W., Deng, X., and Wu, D.: An analysis of aerosol liquid water content and related impact factors in Pearl River Delta, Sci. Total Environ., 579, 1822–1830, https://doi.org/10.1016/j.scitotenv.2016.11.167, 2017.

Tang, I. N. and Munkelwitz, H. R.: Water activities, densities, and refractive indices of aqueous sulfates and sodium nitrate droplets of atmospheric importance, J. Geophys. Res.-Atmos., 99, 18801–18808, https://doi.org/10.1029/94JD01345, 1994.

Tao, J., Kuang, Y., Ma, N., Zheng, Y., Wiedensohler, A., and Zhao, C.: An improved parameterization scheme for size-resolved particle activation ratio and its application on comparison study of particle hygroscopicity measurements between HTDMA and DMA-CCNC, Atmos. Environ., 226, 117403, https://doi.org/10.1016/j.atmosenv.2020.117403, 2020.

Wang, Q., Zhao, J., Du, W., Ana, G., Wang, Z., Sun, L., Wang, Y., Zhang, F., Li, Z., Ye, X., and Sun, Y.: Characterization of submicron aerosols at a suburban site in central China, Atmos. Environ., 131, 115–123, https://doi.org/10.1016/j.atmosenv.2016.01.054, 2016.

Wang, X., Shen, X. J., Sun, J. Y., Zhang, X. Y., Wang, Y. Q., Zhang, Y. M., Wang, P., Xia, C., Qi, X. F., and Zhong, J. T.: Size-resolved hygroscopic behavior of atmospheric aerosols during heavy aerosol pollution episodes in Beijing in December 2016, Atmos. Environ., 194, 188–197, https://doi.org/10.1016/j.atmosenv.2018.09.041, 2018.

Wang, Y., Zhang, F., Li, Z., Tan, H., Xu, H., Ren, J., Zhao, J., Du, W., and Sun, Y.: Enhanced hydrophobicity and volatility of submicron aerosols under severe emission control conditions in Beijing, Atmos. Chem. Phys., 17, 5239–5251, https://doi.org/10.5194/acp-17-5239-2017, 2017.

Wang, Y., Li, Z., Zhang, Y., Du, W., Zhang, F., Tan, H., Xu, H., Fan, T., Jin, X., Fan, X., Dong, Z., Wang, Q., and Sun, Y.: Characterization of aerosol hygroscopicity, mixing state, and CCN activity at a suburban site in the central North China Plain, Atmos. Chem. Phys., 18, 11739–11752, https://doi.org/10.5194/acp-18-11739-2018, 2018.

Weingartner, E., Gysel, M., and Baltensperger, U.: Hygroscopicity of Aerosol Particles at Low Temperatures. 1. New Low-Temperature H-TDMA Instrument: Setup and First Applications, Environ. Sci. Technol., 36, 55–62, https://doi.org/10.1021/es010054o, 2002.

Wu, Z. J., Poulain, L., Henning, S., Dieckmann, K., Birmili, W., Merkel, M., van Pinxteren, D., Spindler, G., Müller, K., Stratmann, F., Herrmann, H., and Wiedensohler, A.: Relating particle hygroscopicity and CCN activity to chemical composition during the HCCT-2010 field campaign, Atmos. Chem. Phys., 13, 7983–7996, https://doi.org/10.5194/acp-13-7983-2013, 2013.

Wu, Z. J., Zheng, J., Shang, D. J., Du, Z. F., Wu, Y. S., Zeng, L. M., Wiedensohler, A., and Hu, M.: Particle hygroscopicity and its link to chemical composition in the urban atmosphere of Beijing, China, during summertime, Atmos. Chem. Phys., 16, 1123–1138, https://doi.org/10.5194/acp-16-1123-2016, 2016.

Xie, Y., Ye, X., Ma, Z., Tao, Y., Wang, R., Zhang, C., Yang, X., Chen, J., and Chen, H.: Insight into winter haze formation mechanisms based on aerosol hygroscopicity and effective density measurements, Atmos. Chem. Phys., 17, 7277–7290, https://doi.org/10.5194/acp-17-7277-2017, 2017.

Xu, B., Zhang, Z.-F., Li, Y.-W., Qin, X., Miao, Q., and Shen, Y.: Hygroscopic Properties of Aerosol Particles in North Suburb of Nanjing in Spring, Huan jing ke xue = Huanjing kexue, 36,

1911–1918, https://doi.org/10.13227/j.hjkx.2015.06.001, 2015 (in Chinese).

Ye, X., Tang, C., Yin, Z., Chen, J., Ma, Z., Kong, L., Yang, X., Gao, W., and Geng, F.: Hygroscopic growth of urban aerosol particles during the 2009 Mirage-Shanghai Campaign, Atmos. Environ., 64, 263–269, https://doi.org/10.1016/j.atmosenv.2012.09.064, 2013.

Yue, D. L., Hu, M., Zhang, R. Y., Wang, Z. B., Zheng, J., Wu, Z. J., Wiedensohler, A., He, L. Y., Huang, X. F., and Zhu, T.: The roles of sulfuric acid in new particle formation and growth in the mega-city of Beijing, Atmos. Chem. Phys., 10, 4953–4960, https://doi.org/10.5194/acp-10-4953-2010, 2010.

Zhang, F., Li, Y., Li, Z., Sun, L., Li, R., Zhao, C., Wang, P., Sun, Y., Liu, X., Li, J., Li, P., Ren, G., and Fan, T.: Aerosol hygroscopicity and cloud condensation nuclei activity during the AC$^3$Exp campaign: implications for cloud condensation nuclei parameterization, Atmos. Chem. Phys., 14, 13423–13437, https://doi.org/10.5194/acp-14-13423-2014, 2014.

Zhang, F., Wang, Y., Peng, J., Ren, J., Collins, D., Zhang, R., Sun, Y., Yang, X., and Li, Z.: Uncertainty in Predicting CCN Activity of Aged and Primary Aerosols, J. Geophys. Res.-Atmos., 122, 11723–11736, https://doi.org/10.1002/2017JD027058, 2017.

Zhang, F., Ren, J., Fan, T., Chen, L., Xu, W., Sun, Y., Zhang, R., Liu, J., Jiang, S., Jin, X., Wu, H., Li, S., Cribb, M. C., and Li, Z.: Significantly Enhanced Aerosol CCN Activity and Number Concentrations by Nucleation-Initiated Haze Events: A Case Study in Urban Beijing, J. Geophys. Res.-Atmos., 124, 14102–14113, https://doi.org/10.1029/2019JD031457, 2019.

Zhang, F., Wang, Y., Peng, J., Chen, L., Sun, Y., Duan, L., Ge, X., Li, Y., Zhao, J., Liu, C., Zhang, X., Zhang, G., Pan, Y., Wang, Y., Zhang, A. L., Ji, Y., Wang, G., Hu, M., Molina, M. J., and Zhang, R.: An unexpected catalyst dominates formation and radiative forcing of regional haze, P. Natl. Acad. Sci. USA, 117, 3960–3966, https://doi.org/10.1073/pnas.1919343117, 2020.

Zhang, J., Wang, L., Chen, J., Feng, S., Shen, J., and Jiao, L.: Hygroscopicity of ambient submicron particles in urban Hangzhou, China, Front. Environ. Sci. En., 5, 342–347, 2011.

Zhang, S. L., Ma, N., Kecorius, S., Wang, P. C., Hu, M., Wang, Z. B., Größ, J., Wu, Z. J., and Wiedensohler, A.: Mixing state of atmospheric particles over the North China Plain, Atmos. Environ., 125, 152–164, https://doi.org/10.1016/j.atmosenv.2015.10.053, 2016.

Zhao, J., Du, W., Zhang, Y., Wang, Q., Chen, C., Xu, W., Han, T., Wang, Y., Fu, P., Wang, Z., Li, Z., and Sun, Y.: Insights into aerosol chemistry during the 2015 China Victory Day parade: results from simultaneous measurements at ground level and 260 m in Beijing, Atmos. Chem. Phys., 17, 3215–3232, https://doi.org/10.5194/acp-17-3215-2017, 2017.

Zhong, H., Huang, R.-J., Chang, Y., Duan, J., Lin, C., and Chen, Y.: Enhanced formation of secondary organic aerosol from photochemical oxidation during the COVID-19 lockdown in a background site in Northwest China, Sci. Total Environ., 778, 144947, https://doi.org/10.1016/j.scitotenv.2021.144947, 2021.